Supporting Information for:

Acoustic Vibrations of Au Nano-Bipyramids and their Modification under Ag Deposition: a Perspective for the Development of Nanobalances

Benoît Dacosta Fernandes[1], Miguel Spuch-Calvar[2], Hatim Baida[1], Mona Tréguer-Delapierre[2], Jean Oberlé[1], Pierre Langot[1] and Julien Burgin[1]

1 Univ. Bordeaux, LOMA, UMR 5798, F-33400 Talence, France

2 CNRS, ICMCB, UPR 9048, F-33600 Pessac, France

A – Intrinsic damping time determination

Our measurements are performed in colloidal solution, we thus probe the vibrations of a large ensemble of nanoparticles. Consequently, the polydispersity of the sample yields an inhomogeneous contribution on damping. When fitting with the following equation,

$$f(t) = \sum_i A_i e^{-t/\tau_i} \cos\left(\frac{2\pi}{T_i} t + \varphi_i\right) + B\, e^{-t/\tau_{bg}}$$

, the measured damping time for the mode i (τ_i) contains an intrinsic contribution ($\tau_{i,h}$) and an inhomegeneous contribution (τ_i^*) related to the particle size distribution. To determine the intrinsic damping time, we need to remove the inhomogeneous contribution. To achieve this task, we need to consider the size distribution of the particles (mean length L_m and standard deviation σ_L). For samples with a weak standard deviation ($\sigma_L \ll L_m$), we can assume that the vibrational period depends linearly with the length of the bipyramids and define the standard deviation of the vibrational period from the length standard deviation: $\frac{\sigma_T}{T} = \frac{\sigma_L}{L_m}$. For our samples, these ratios are estimated around 5%. Moreover, in the weak standard deviation regime, we can also approximate the inhomogeneous damping time by $\tau_i^* \approx {T_i^2}\Big/{\sqrt{2\pi}\sigma_T}$ and then estimate the homogeneous damping time τ_h by fitting the signal with the following equation:[1,2]

$$g(t) = \sum_i A_i\, e^{-(t/\tau_i^*)^2}\, e^{-t/\tau_{i,h}} \cos\left(\frac{2\pi}{T_i} t + \varphi_i\right) + B\, e^{-t/\tau_{bg}}$$

Note here we only performed the estimation on the fundamental mode because the results are not representative for other modes which present weak signals. To estimate the quality factor, we thus calculated $Q = \pi \frac{\tau_{i,h}}{T_i}$ for the fundamental extensional mode for core samples and core shell samples CSa, CSb and CSc. The results are presented on Figure 1 as a function of the length.
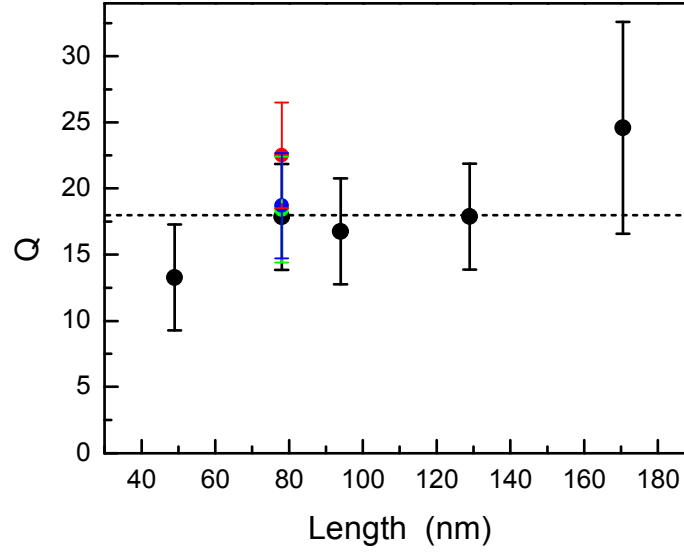
Figure 1. Quality factor of the fundamental extensional mode measured in several core samples as a function of the nano-bipyramid length. The coloured dots correspond to the core shell samples (CSa, CSb and CSc). The dotted line corresponds to the average.

We see that the quality factor measure for the fundamental extensional mode is barely constant and found to be close to the measure in identical particles nm 79 nm long (note here one need to remove the fluid component to determine the intrinsic quality factor values).[2] Further investigation and discussion would necessitate single particles measurements.[3]

For the core shell samples, we found the following values: 22.5 for CSa, 18.4 for CSb and 18.7 for CSc. These values are quite close to the one measured in the core particle on which they are synthesized (Q_{core} = 18.3).

B –Finite element analysis

We performed finite element analysis using COMSOL software: Solid mechanics module, Eigen frequency solver. We calculated the vibration Eigen modes frequencies of 3D solids or we used the 2D axisymmetry mode to reduce the calculus times when possible. We used the elastic constants of bulk polycrystalline gold (Young's modulus E = 78.5 GPa, Poisson's ratio υ=0.42 and ρ = 19 300 kg.m^{-3}) or silver (E = 83 GPa, υ=0.36 and ρ = 10 490 kg.m^{-3}).

B-1 Periods for core-shell particles

To clarify the complex behavior of the calculated periods for bicones as a function of the size parameter γ, we also calculated the periods for pure metal particle (gold or silver) for an identical shape. For the Au-Ag core-shell, the core is designed with two triangles, yielding a simple bicone and the shell is delimited by a radius ρ depending on the altitude z varying between $-L/2$ and $L/2$, $\rho(z) = e_2 + \frac{D}{2} \left(1 - \left(\frac{z}{\frac{L}{2}+e_1} \right)^{\gamma} \right)^{1/\gamma}$. For the pure Au or Ag particles, the shape is simply delimited by $\rho(z)$.
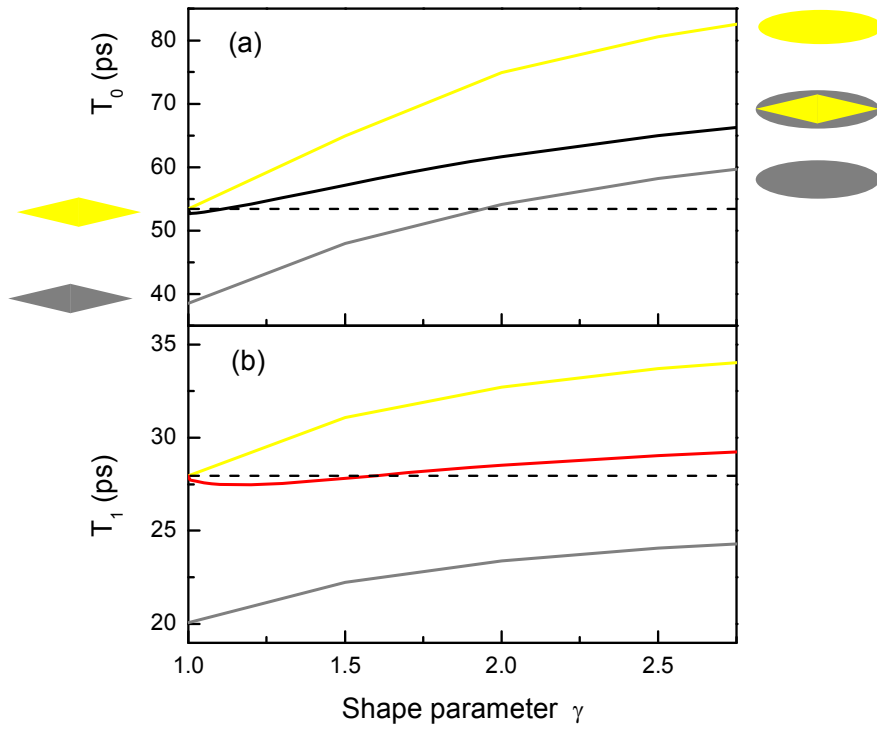

Figure 2. Computed periods of the fundamental extensional mode (a) and its first harmonic (b), for Au-Ag core-shell particle (black), pure Au (yellow) and pure Ag (grey) as a function of the shape parameter γ. The dotted line corresponds to the period of the core biconical reference particle (L=100nm, D=30 nm, γ=1).

The pure Au or Ag particles present the same behaviour: the periods increase when γ increases, which can be simply associated to a mass increase of the particle. We also remark that the periods are smaller in silver which is expected if we consider its elastic constants. For

core-shell particles, we observe a more complex behaviour that is not a simple average but is in between pure Au and Ag particles. This kind of behaviour has also been observed in Au-Pd particles in relatively similar geometries and has been associated to stiffening and mass addition effects.[4] The decrease of the period for small γ values is present when stiffening dominates whereas the increase of the periods for larger γ values reflects the addition of mass. Notice here that the periods does not strongly converge on our plot because we studied small variations of shape; stronger modifications of the particles (increasing e_1 or e_2) would result in the convergence of the periods for Au-Ag core-shell and pure Ag particles, as it has been evidenced in Au-Pt rods.[4]

B-2 Amplitudes for core and core-shell particles

To estimate the amplitude of excitation of the different modes, we calculated the projection of the initial condition (dilatation) displacement field (X,Y,Z) onto the orthogonal basis of calculated vibrational modes displacement field (u,v,w).[5,6] We calculated the following normalized scalar product for every mode i :

$$A_i^{exc} = \frac{\iiint \rho(u_i * X + v_i * Y + w_i * Z)\ dV}{\sqrt{\iint \rho(u_i * u_i + v_i * v_i + w_i * w_i)dV}\ \sqrt{\iint \rho(X * X + Y * Y + Z * Z)dV}}$$

, where ρ correspond to the volume mass of the medium. A_i^{exc} correspond to the excitation amplitude. Note that this calculation does not include the influence of the detection mechanism over the amplitude.[5]

In the following discussion, we will principally focus on A_0 the excitation amplitude of the fundamental extensional mode, A_1 the excitation amplitude is first harmonic and A_{rad} the excitation amplitude of the radial mode.

We firstly investigated the shape of the core particle. We performed calculations for four kinds of core particles: with a circular section (bicone) or a pentagonal section (bipyramid) and with a sharp tip or a rounded tip. The figure 2 presents the two more realistic core shapes (a-b), *i.e.* shapes with a rounded tip. The determination of the periods is not strongly affected by these details (<3%) but we find that they impact the amplitudes. We will focus the discussion using the results of calculations based on bipyramids with a pentagonal section and a rounded tip (Figure2, shape b), *i.e.* the more realistic shape.
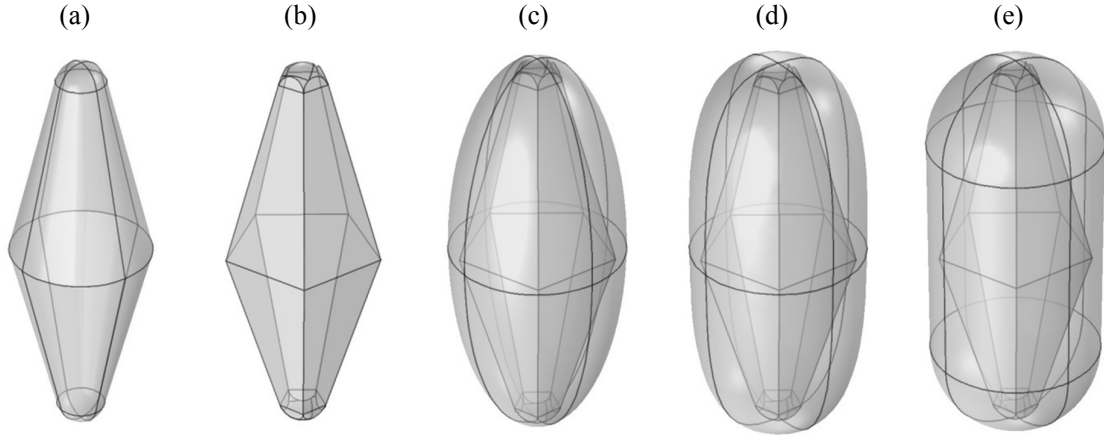
Figure 3. 3D shapes of the particle used for finite element analysis calculation of amplitudes (a) Core bicone (Length=78 nm, Diameter = 28 nm, tip radius r = 5 nm). (b) Core pentagonal bipyramids (L=78 nm, D = 28 nm, tip radius r = 5 nm) on which the core-shell shapes are built. (c) Core-shell particle made with an ellipsoidal shape (γ=2). (d) Core-shell particle made with the parameterized shape (γ=3). (e) Core-shell particle made with a cylindrical shape, ended by a sphere. The length of the core-shell particles are L = 79 nm and D = 34 nm, (corresponding to e_1 = 0.5 nm and e_2 = 3 nm).

The figure 4 presents the excitations amplitudes ad a function of the mode frequency for the core shape (a) and shape (b). We see that the amplitudes A_0 and A_1 are weakly modified by the transverse geometry (Table 1), whereas the radial mode amplitude (frequency around 100 GHz) is quenched by a factor ~2. Note also the apparition of a new mode at frequency ~108GHz for the pentagonal shape (b) (Figure 4b). This mode may correspond to an hybrid mode, already observed and simulated in single gold nanowires.[6] The study of this fine feature is further than the scope of the present study and necessitates single particle measurements. Finally, we also calculate the excitation amplitude in rounded cylinder in order to mimic nanorods. We find that the first harmonic mode is weakly excited whereas the radial mode is well excited in this geometry (as observed in experiments).[7]
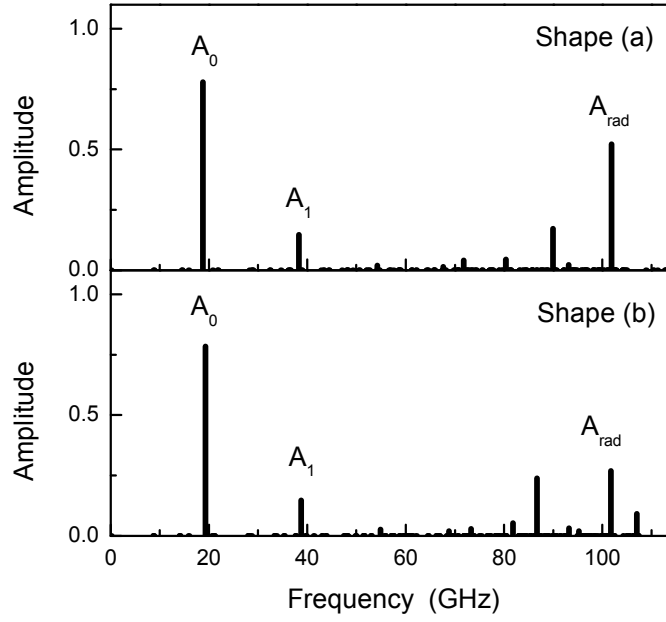
Figure 4. Excitation amplitude of the vibrational modes versus the frequency for the rounded bicone (a) and rounded pentagonal bipyramid (b).

Shape	$(A_1/A_0)^{core}$	$(A_{rad}/A_0)^{core}$
(a)	0.188	0.668
(b)	0.186	0.342
Rounded cylinder	0.0058	0.684

Table 1. Ratio of the excitation amplitudes of several modes for two core particle shapes (a and b) and a rounded cylinder. The sizes are L = 79 nm, D = 34 nm, r=5nm.

Secondly, we calculated the amplitudes for core-shell particles with several kinds of shell (Table 2). The investigated shell are presented on the figure 3. The shapes (c) and (d) are built with the γ-parametrized function $\rho(z)$ for $\gamma=2$ (ellipsoid) and $\gamma=3$ respectively. The shape (d) is a bit different; it is made of a rounded cylinder embedding the core. These calculations show an enhancement of the radial mode and a quenching of the first harmonic in core-shell particles and discussed in the main article. We added data illustrating the impact of γ (Shapes c, c1 and d) and the impact of shell thickness lateral of e_2 (2, 3 and 4 nm for the shapes d, d1 and d2).
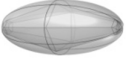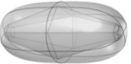
Shell Shape (pentagonal)	$(A_1/A_0)^{CS}$	$\dfrac{(A_0/A_1)^{CS}}{(A_0/A_1)^{core}}$	$(A_{rad}/A_0)^{CS}$	$\dfrac{(A_{rad}/A_0)^{CS}}{(A_{rad}/A_0)^{core}}$
(b) D = 28 nm	0.186	1	0.342	1
(c) γ=2 / 34nm	0.181	1.04	0.838	2.45
(c1) γ=2.5 / 34nm	0.139	1.34	0.720	2.1
(d) γ=3 / 34nm	0.115	1.62	0.646	1.89
(d1) γ=3 / 32nm	0.122	1.52	0.503	1.47
(d2) γ=3 / 36nm	0.107	1.73	0.647	1.90

Table 2. Ratio of the excitation amplitudes of several modes for core pentagonal bipyramids (b) and five γ parameterized shells based on this core. The length indicated corresponds to the total core-shell diameter.

These calculations confirm the measured trends but fail to predict exactly the amplitudes. The origin of this discrepancy can be discussed. Firstly, a very fine correspondence between the particles real shape and their numerical model should improve the agreement, but it will probably be done combining 3D TEM tomography and single particle measurements. Secondly, since we calculate the excitation amplitudes without considering the detection mechanism (and thus the detection efficiency), it is reasonable to think discrepancies originate from this issue. Very few studies have addressed this problem because they are a numerical challenge, especially for complex shapes. Meanwhile, this issue has been addressed in the spherical geometry.[5,8,9] For this simple geometry, the fundamental breathing mode and its harmonics have been studied and the following expression of the amplitudes ratio have been found: $\frac{A_0^{total}}{A_1^{total}} = \frac{A_0^{exc}}{A_1^{exc}} \sqrt{\frac{T_0}{T_1}} \frac{u_0}{u_1}$, u being the displacement field at the surface.[9] If we roughly consider our systems follow this dependency, we can correct the calculated ratio A_{rad}/A_0 by a factor ~0.4 and the ratio A_1/A_0 by a factor ~ 0.7 for core particles. Moreover, this term slightly affects (~4%) the evolution of the ratio $\frac{(A_{rad}/A_0)^{core-shell}}{(A_{rad}/A_0)^{core}}$ because the effect is compensated. Concerning the effect of the displacement field ratio, we prefer not to discuss it here (lack of relevance); the impact of the anisotropic shape of the particle and the displacement fields of the modes on the detection efficiency should be addressed carefully, which is not easily reachable and is further the scope of this study.

References

[1] G. V. Hartland, Coherent Vibrational Motion in Metal Particles: Determination of the Vibrational Amplitude and Excitation Mechanism, *J. Chem. Phys.* **2002**, 116, 8048-8055.

[2] M. Pelton, J. Sader, J. Burgin, M. Liu, P. Guyot-Sionnest and D. Gosztola, Damping of Acoustic Vibrations in Gold Nanoparticles, *Nat. Nanotechnol.* **2009**, 4, 492-495.

[3] P. V. Ruijgrok, P. Zijlstra, A. L. Tchebotareva and M. Orrit, Damping of Acoustic Vibrations of Single Gold Nanoparticles Optically Trapped in Water, *Nano Lett.* **2012**, 12, 1063-1069.

[4] M. F. Cardinal, D. Mongin, A. Crut, P. Maioli, B. Rodríguez-González, J. Pérez-Juste, L. M. Liz-Marzán, N. Del Fatti and F. Vallée, Acoustic Vibrations in Bimetallic Au@Pd Core–Shell Nanorods, *J. Phys. Chem. Lett.* **2012**, 3, 613-619.

[5] A. Crut, V. Juvé, D. Mongin, P. Maioli, N. Del Fatti and F. Vallée, Vibrations of Spherical Core-Shell Nanoparticles, *Phys. Rev. B* **2011**, 83, 205430-209439.

[6] T. A. Major, A. Crut, B. Gao, S. S. Lo, N. Del Fatti, F. Vallée and G. V. Hartland, Damping of the Acoustic Vibrations of a Suspended Gold Nanowire in Air and Water Environments, *Phys. Chem. Chem. Phys.* **2013**, 15, 4169-4176.

[7] P. Zijlstra, A. L. Tchebotareva, J. W. M. Chon, M. Gu and M. Orrit, Acoustic Oscillations and Elastic Moduli of Single Gold Nanorods, *Nano Lett.* **2008**, 8, 3493-3497.

[8] A. Nelet, A. Crut, A. Arbouet, N. Del Fatti, F. Vallée, H. Portalès, L. Saviot, and E. Duval, Acoustic Vibrations of Metal Nanoparticles: High Order Radial Mode Detection, *Appl. Surf. Sci.* **2004**, 226, 209-215.

[9] A. Arbouet, N. Del Fatti, and F. Vallée, Optical Control of the Coherent Acoustic Vibration of Metal Nanoparticles, *J. Chem. Phys.* **2006**, 124, 144701-144704.